Acta Pharmacologica Sinica

ARTICLE

Reduced intracellular chloride concentration impairs angiogenesis by inhibiting oxidative stress-mediated VEGFR2 activation

Kai Li[2], Ying-ying Liu[2], Xiao-fei Lv[2], Zhuo-miao Lin[2], Ting-ting Zhang[2], Fei-ran Zhang[2], Jia-wei Guo[2], Yu Hong[2], Xiu Liu[2], Xiao-chun Lin[2], Jia-guo Zhou[1,2,3,4,5,6], Qian-qian Wu[7,8,9], Si-jia Liang[1,2] and Jin-yan Shang[1,2]

Chloride (Cl^-) homeostasis is of great significance in cardiovascular system. Serum Cl^- level is inversely associated with the mortality of patients with heart failure. Considering the importance of angiogenesis in the progress of heart failure, this study aims to investigate whether and how reduced intracellular Cl^- concentration ($[Cl^-]_i$) affects angiogenesis. Human umbilical endothelial cells (HUVECs) were treated with normal Cl^- medium or low Cl^- medium. We showed that reduction of $[Cl^-]_i$ (from 33.2 to 16.18 mM) inhibited HUVEC proliferation, migration, cytoskeleton reorganization, tube formation, and subsequently suppressed angiogenesis under basal condition, and VEGF stimulation or hypoxia treatment. Moreover, VEGF-induced NADPH-mediated reactive oxygen species (ROS) generation and VEGFR2 axis activation were markedly attenuated in low Cl^- medium. We revealed that lowering $[Cl^-]_i$ inhibited the expression of the membrane-bound catalytic subunits of NADPH, i.e., p22phox and Nox2, and blunted the translocation of cytosolic regulatory subunits p47phox and p67phox, thereby restricting NADPH oxidase complex formation and activation. Furthermore, reduced $[Cl^-]_i$ enhanced ROS-associated protein tyrosine phosphatase 1B (PTP1B) activity and increased the interaction of VEGFR2 and PTP1B. Pharmacological inhibition of PTP1B reversed the effect of lowering $[Cl^-]_i$ on VEGFR2 phosphorylation and angiogenesis. In mouse hind limb ischemia model, blockade of Cl^- efflux using Cl^- channel inhibitors DIDS or DCPIB (10 mg/kg, i.m., every other day for 2 weeks) significantly enhanced blood flow recovery and new capillaries formation. In conclusion, decrease of $[Cl^-]_i$ suppresses angiogenesis via inhibiting oxidase stress-mediated VEGFR2 signaling activation by preventing NADPH oxidase complex formation and promoting VEGFR2/PTP1B association, suggesting that modulation of $[Cl^-]_i$ may be a novel therapeutic avenue for the treatment of angiogenic dysfunction-associated diseases.

Keywords: chloride; angiogenesis; oxidative stress; VEGFR2; PTP1B; PTP1B inhibitor II

Acta Pharmacologica Sinica (2021) 42:560–572; https://doi.org/10.1038/s41401-020-0458-7

INTRODUCTION

Angiogenesis is characterized by new capillary formation from preexisting vessels and plays an important role in regulating various diseases, such as myocardial infarction, stroke, wound healing, diabetic retinopathy, neurodegenerative disorders, and tumors [1–3]. The sprouting of new blood vessels is triggered by dissolution of the vascular basal membrane and degradation of the extracellular matrix followed by endothelial cell migration, invasion, proliferation, and tube formation [4]. A low level of reactive oxygen species (ROS) was shown to be essential for cellular homeostasis [5]. Regarding vascular endothelial cells, physiological angiogenesis is paralleled by a low level of oxidative stress [6]. In response to multiple stress factors, such as growth factors, tissue ischemia/hypoxia, and ischemic preconditioning, ROS function as important signaling molecules, for example, by regulating phospho-tyrosine phosphatases (PTPs) activity, which is associated with vascular endothelial growth factor receptor 2 (VEGFR2), to mediate endothelial cell proliferation and migration during angiogenesis [7].

Vascular endothelial growth factors (VEGFs) have been proposed to be crucial regulators of angiogenesis that influence vascular development and vasculature growth [8]. The VEGF family comprises seven members: VEGF (or VEGF-A), VEGF-B, VEGF-C, VEGF-D, VEGF-E, VEGF-F, and placental growth factor [9]. VEGF-A has become a major research focus because of its specific and prominent angiogenic function among all members [1, 10]. In intact endothelial cells, the function of VEGF-A is primarily

[1]Program of Kidney and Cardiovascular Disease, The Fifth Affiliated Hospital, Sun Yat-Sen University, Zhuhai 519000, China; [2]Department of Pharmacology, Cardiac and Cerebral Vascular Research Center, Zhongshan School of Medicine, Sun Yat-Sen University, Guangzhou 510080, China; [3]Guangdong Province Key Laboratory of Brain Function and Disease, Zhongshan School of Medicine, Sun Yat-Sen University, Guangzhou 510080, China; [4]Department of Cardiology, Sun Yat-sen Memorial Hospital, Sun Yat-Sen University, Guangzhou 510080, China; [5]Department of Physiology, Key Laboratory of Cardiovascular disease, School of Basic Medical Sciences, Guangzhou Medical University, Guangzhou 511436, China; [6]Guangzhou Institute of Cardiovascular Disease, The Second Affiliated Hospital, Guangzhou Medical University, Guangzhou 511436, China; [7]Key Laboratory of Metabolic Cardiovascular Diseases Research of National Health Commission, Ningxia Medical University, Yinchuan 750004, China; [8]Ningxia Key Laboratory of Vascular Injury and Repair Research, Ningxia Medical University, Yinchuan 750004, China and [9]School of Basic Medical Sciences, Ningxia Medical University, Yinchuan 750004, China
Correspondence: Jin-yan Shang (shangjy5@mail.sysu.edu.cn) or Si-jia Liang (liangsj5@mail.sysu.edu.cn)
These authors contributed equally: Kai Li, Ying-ying Liu, Xiao-fei Lv

Received: 10 November 2019 Accepted: 7 June 2020
Published online: 21 July 2020

mediated by binding to VEGFR2, leading to VEGFR2 dimerization and strong ligand-dependent tyrosine phosphorylation [11]. Upon VEGF/VEGFR2 activation, downstream signaling pathways, such as the PI3K, AKT, PLCγ1, p38, and ERK1/2 pathways, result in angiogenic signal transduction and subsequent endothelial cell chemotaxis and proliferation [1, 12].

Chloride (Cl^-) is the primary anion in extracellular fluid. Cl^- movement across the cell plasma membrane plays a key role in regulating cell volume, proliferation, apoptosis, neuron excitability, and synaptic transmission [13, 14]. Previous work from our laboratory and others has shown an obvious change in the intracellular Cl^- concentration ($[Cl^-]_i$) of T cells undergoing apoptosis, of hippocampal neurons during development, and of macrophages from patients with hypercholesterolemia or atherosclerotic ApoE$^{-/-}$ mice [15–18]. Moreover, we showed that a decrease in $[Cl^-]_i$ could potentiate endothelial cell inflammation, vascular smooth muscle cell proliferation, and macrophage foam cell formation [14, 18, 19]. These findings suggest that $[Cl^-]_i$ plays an essential role in maintaining cardiovascular homeostasis. Importantly, recent studies have reported that a decrease in serum Cl^- concentration is associated with an increased risk of mortality in patients with hypertension, myocardial infarction, or heart failure, indicating that serum Cl^- concentration is an independent predictor of the outcome of patients with cardiovascular diseases [2, 20, 21]. Notably, heart failure is frequently associated with collagen breakdown and reduced angiogenesis [22]. Targeting angiogenesis has emerged as an attractive therapeutic option for the treatment of heart failure [3, 23]. Thus, reduced $[Cl^-]_i$ may impair angiogenesis in ischemic diseases, such as heart failure.

The present study aims to investigate the effect of lowering $[Cl^-]_i$ on angiogenesis in endothelial cells using low Cl^- medium. Our results demonstrated that reduction of $[Cl^-]_i$ suppresses NADPH oxidase-mediated ROS generation and consequently increases protein tyrosine phosphatase 1B (PTP1B) activity, thus inhibiting VEGFR2 activation and angiogenesis. Inhibition of Cl^- efflux with volume-regulated anion channel (VRAC) blockers facilitated revascularization of the ischemic hind limb in mice.

MATERIALS AND METHODS

Antibodies and reagents

Antibodies against VEGFR2 (#2479), phospho-VEGFR2 (Tyr951) (#4991), phospho-VEGFR2 (Tyr1059) (#3817), phospho-VEGFR2 (Tyr1175) (#3770), PLCγ1 (#5690), phospho-PLCγ1 (Tyr783) (#2821), ERK1/2 (#4695), phospho-ERK (Thr202/Tyr204) (#4370), AKT (#9272), phospho-AKT (S473) (#4060), PI3K (#4292), phospho-PI3K (Tyr458) (#4228), Src (#2109), phospho-Src (Tyr416) (#2101), FAK (#3285), phospho-FAK (Tyr397) (#3283), p38 (#9212), phospho-p38 (Thr180/Tyr182) (#4631), and PTP1B (#5311) were obtained from Cell Signaling Technology (Beverly, MA, USA). Phospho-VEGFR2 (Tyr1214) (TA311979) was purchased from Origene (Rockville, MD, USA). Paxillin (10029-1-Ig), vinculin (66305-1-Ig) and GAPDH (60004-1-Ig) antibodies were obtained from Proteintech Group (Rosemont, IL, USA). Antibodies against p22phox (sc-271262), p47phox (sc-17845), p67phox (sc-374510), Rac1 (sc-217), and Na^+-K^+-ATPase (sc-71638), Protein G beads and IgG were purchased from Santa Cruz Biotechnology (Dallas, TX, USA). Phospho-p47phox (ab111855) antibody was purchased from Abcam (Cambridge, MA, USA). Recombinant human VEGF, DAPI dye, rhodamine-phalloidin, 4,4′-diisothiocyanatostilbene-2,2′-disulfonic acid disodium salt hydrate (DIDS), 2′,7′-dichlorofluorescin diacetate (H_2DCF-DA), dihydroethidium (DHE), lucigenin, NADPH, p-nitrophenyl phosphate (pNPP), and 4-[(2-butyl-6,7-dichloro-2-cyclopentyl-2,3-dihydro-1-oxo-1H-inden-5-yl)oxy]butanoic acid (DCPIB) were obtained from Sigma-Aldrich (St. Louis, MO, USA). PTP1B inhibitor II was obtained from MedChem Express (Monmouth Junction, NJ, USA).

Aortic ring assay

C57/BL6 mice (weighing ~20 g and aged 8–10 weeks) were obtained from the Animal Center of Sun Yat-sen University (Guangzhou, Guangdong, China). All animal study protocols conformed to the 'Guide for the Care and Use of Laboratory Animals' of the National Institute of Health in China and were approved by the Animal Ethical and Welfare Committee of Sun Yat-sen University. The aortic ring assay was performed as described previously with some modifications [24]. Briefly, 48-well plates were covered with 100 μL of Matrigel (BD Biosciences, San Diego, CA, USA) and incubated at 37 °C and 5% CO_2 for 30 min. Mice were anesthetized with 2% pentobarbital sodium, and the aortas were dissected. After the periadventitial fat and connective tissues were carefully cleaned, the aortas were cut into ~1–1.5-mm-long rings and placed on Matrigel-covered wells. The aortic rings were cultured in serum-free medium for 24 h, and then, the medium was replaced with normal Cl^- medium or low Cl^- medium in the absence or presence of VEGF (50 ng/mL). The medium was changed every 2 days with the exact composition as mentioned above. After 4 days, microvessel growth was observed using an inverted microscope (TH4-200, Olympus, Tokyo, Japan). The outgrowth area was delineated and quantified with Image-Pro Plus software (Version 6.0, Meyer Instruments, Houston, TX, USA).

Cell isolation and culture

Human umbilical endothelial cells (HUVECs) were isolated as previously described [19, 25]. HUVECs were cultured in medium 199 (M199) containing penicillin (100 U/mL)-streptomycin (100 U/mL), 20% heat-inactivated fetal bovine serum (FBS), *L*-glutamine (2 mmol/L), heparin (25 U/mL), and basic fibroblast growth factor (5 ng/mL) (all from Invitrogen, Carlsbad, CA, USA). Cultures were maintained in a humidified chamber at 37 °C containing 95% O_2 plus a 5% CO_2 atmosphere. Culture experiments were performed at 37 °C with 5% CO_2 under normoxic (21% O_2) or hypoxic (1% O_2) conditions.

Preparation of low Cl^- medium

The low Cl^- medium was prepared as previously described [18, 19]. Briefly, the M199 cell culture medium lacking KCl and NaCl, which accounted for 99.5% of the total Cl^- content, was initially obtained from Invitrogen. The normal chloride medium was prepared by addition of 5 mmol/L KCl and 105 mmol/L NaCl. The low Cl^- medium was prepared by addition of 5 mmol/L potassium gluconate and 105 mmol/L sodium gluconate. The osmolarities of the solutions ranged between 303.4 and 310.2 mosmol/kg·H_2O and were measured by a freezing point depression osmometer (Osmomat 030, Germany).

Cell viability assay

The viability of HUVECs was determined by CCK-8 assays (Dojindo Laboratories, Kumamoto, Japan). In brief, HUVECs were seeded in 96-well plates at a density of 5×10^4 cells/well. Twenty-four hours later, the cells were treated with normal Cl^- or low Cl^- medium containing VEGF (50 ng/mL) for 48 h. Then, the cells were incubated with 10 μL of CCK-8 reagent for 4 h at 37 °C and 5% CO_2. The absorbance was determined at 540 nm using a microplate reader (Bio-Tek, VY, USA).

Migration assay

Cell migration was assessed by Transwell analysis using a modified Boyden chamber with 8-μm pore size polycarbonate filters (Millipore, Beverly, MA, USA) as described previously [24]. Normal Cl^- or low Cl^- medium containing 0.5% FBS was added to the lower well in the absence or presence of VEGF (50 ng/mL). HUVECs (5×10^4 cells/well) were seeded in the upper chambers and incubated at 37 °C in a 95% O_2 and 5% CO_2 atmosphere. Twenty-four hours later, the unmigrated cells were removed using cotton swabs. The migrated cells were fixed with 4% paraformaldehyde for 20 min and

stained with 0.2% crystal violet in 10% ethanol. The stained cells were observed and counted using a microscope (IX71, Olympus).

Tube formation assay

Ninety-six-well plates were coated with 60 μL of Matrigel at 37 °C for 30 min. HUVECs (5×10^4 cells/well) were harvested and suspended in normal Cl^- or low Cl^- medium with or without VEGF (50 ng/mL), plated on the polymerized Matrigel and cultured at 37 °C for 48 h. Tube-like structures were photographed using microscopy. The number of tubes was counted in eight random microscope fields, and the lengths of the enclosed tube network were measured by Image-Pro Plus software (Media Cybernetics, Inc., Rockville, MD, USA).

Detection of intracellular ROS generation

Intracellular ROS generation was assessed by H_2DCFDA and DHE staining. Briefly, HUVECs in normal Cl^- or low Cl^- culture medium were treated with or without VEGF (50 ng/mL) for 48 h. Cells were washed with warm PBS and then incubated at 37 °C with H_2DCFDA (10 μmol/L) or DHE (10 μmol/L) in the dark for 30 min in phenol-red free M199. Cells were photographed under a fluorescent microscope (IX71, Olympus, Hamburg, Germany) at 485-nm excitation and 535-nm emission wavelengths for dichlorofluorescein (DCF) and at 535-nm excitation and 610-nm emission wavelengths for DHE. The fluorescence intensity was quantified with ImageJ software (Version 1.41, NIH, Bethesda, MD, USA).

Subcellular fraction isolation

Subcellular fractions as membrane and cytosolic proteins were obtained using a Qproteome Cell Compartment Kit (Qiagen, Valencia, CA) according to the manufacturer's protocol. In brief, the cell suspension was rinsed with PBS and then lysed with ice-cold extraction buffer CE1 for the cytoplasm and ice-cold extraction buffer CE2 for the membrane.

NADPH oxidase activity assay

The NADPH oxidase activity of the cell membrane was measured using a lucigenin-enhanced chemiluminescence assay according to the manufacturer's protocol. After stimulation, the cells were lysed in phosphate buffer (50 mmol/L KH_2PO_4, 1 mmol/L EGTA, 150 mmol/L sucrose and protease inhibitor cocktail, pH 7.0), sonicated for 6 s on ice and centrifuged at $28,000 \times g$ for 15 min at 4 °C. The membrane precipitate was resuspended and incubated with lucigenin (5 μmol/L) and NADPH (100 μmol/L) at 37 °C for 15 min. The light emission was recorded every 15 s for 20 min in a luminometer (MGM Instruments, Hamden, CT, USA). Background counts determined in cell-free preparations were subtracted from the total count. The NADPH oxidase activity was calculated from the ratio of mean light units to the total protein level and is expressed as relative light units (RLU)/s/mg protein.

PTP1B activity assay

PTP1B activity was detected as previously described [26]. Briefly, HUVECs were snap-frozen in liquid nitrogen and disrupted by scraping into ice-cold, deoxygenated homogenization buffer (in mmol/L, 150 NaCl, 5 EDTA, 5 EGTA, 50 HEPES, pH 7.5) containing protease inhibitor, 1% (v/v) Triton X-100, and 0.5% (v/v) NP-40. The whole-cell lysate was cleared by centrifugation at $15,000 \times g$ for 20 min. Specific PTP1B activity was measured by the hydrolysis of pNPP in PTP1B immunoprecipitates. PTP1B immunoprecipitates from 500 μg of cell lysates were incubated in a final volume of 100 μL at 37 °C for 30 min in reaction buffer (in mmol/L, 10 pNPP, 2 EDTA, 20 MES, pH 6.0). The reaction was stopped by the addition of 200 μL of 5 mol/L NaOH, and the absorption was detected at 410 nm on a plate reader (Spectramax190 from Molecular Devices).

Western blotting and immunoprecipitation

HUVECs were lysed in RIPA lysis buffer (Beyotime, Shanghai, China) supplemented with proteinase inhibitor and phosphatase inhibitor. The cell homogenates were centrifuged at $12,000 \times g$ and 4 °C for 15 min, and then, the supernatants were collected. Protein concentration was determined by BCA Protein Assay Reagent (Thermo Scientific, Pittsburgh, PA, USA). Equal amounts of protein were separated by SDS-polyacrylamide gel electrophoresis and transferred onto 0.45-mm PVDF membranes (Millipore). The membranes were blocked with 5% nonfat milk for 1 h and then incubated with appropriate primary antibodies at 4 °C overnight. Then, the blots were visualized with horseradish peroxidase-conjugated secondary antibodies (Beyotime) followed by enhanced chemiluminescence (Millipore). Image quantification was performed using ImageJ software. For immunoprecipitation, equal amounts of protein were incubated with the appropriate primary antibodies followed by immunoprecipitation with protein A/G agarose beads (Santa Cruz Biotechnology, Dallas, TX, USA). The immunoprecipitates were extensively washed with ice-cold PBS and resolved in RIPA lysis buffer. The amounts of bound proteins in immunocomplexes were determined by Western blotting.

Immunofluorescence staining

Immunofluorescence staining was performed using standard techniques on endothelial cell monolayers as previously described [25]. Briefly, HUVECs after treatment were fixed with 4% formaldehyde for 30 min, permeabilized with 0.1% Triton X-100 in PBS for 3 min, blocked with 5% bovine serum albumin in PBS for 1 h at room temperature and then incubated with paxillin and vinculin antibodies (1:100 dilution) at 4 °C overnight. After three washes with PBS, the cells were incubated with Green Donkey Anti-Mouse IgG antibody (1:100 dilution) (A24211) (Abbkine, Wuhan, Hubei, China) for 1 h at 37 °C. F-actin was visualized by rhodamine-phalloidin staining. Images were captured by a laser confocal inverted microscope (BX51, Olympus).

$[Cl^-]_i$ measurement

$[Cl^-]_i$ was measured with 6-methoxy-N-ethylquinolinium iodide (MEQ) as we described previously [18, 19]. In brief, MEQ was reduced to a cell-permeable derivative, 6-methoxy-N-ethyl-1,2-dihydroquinoline (dihydro-MEQ), which was added to cells at a concentration of 150 μmol/L in Ringer's buffer solution (in mmol/L, 119 NaCl, 2.5 KCl, 1.0 NaH_2PO_4, 1.3 $MgSO_4$, 2.5 $CaCl_2$, 26 $NaHCO_3$, 11 glucose, pH 7.4) in the dark at room temperature for 30 min. Then, dihydro-MEQ was quickly oxidized to MEQ in the cytoplasm. The fluorescence of MEQ is quenched collisionally by Cl^-. $[Cl^-]_i$ was monitored by MetaFluor Imaging software (Universal Imaging Systems, Chester, PA, USA) with A 350-nm excitation wavelength and A 435-nm emission wavelength. The relationship between the fluorescence intensity of MEQ and THE chloride concentration is given by the Stern–Volmer equation: $(F_0/F) - 1 = K_{SV}[Q]$, where F_0 is the fluorescence intensity without halide or other quenching ions, F is the fluorescence intensity in the presence of quencher, $[Q]$ is the concentration of quencher, and K_{SV} is the Stern–Volmer constant.

Model of hind limb ischemia

A model of unilateral hind limb ischemia was established by ligation of the femoral artery as previously described [27]. In brief, mice were anesthetized by intraperitoneal injection of pentobarbital sodium. The femoral artery was isolated and then ligated at two positions, one just proximal to the groin ligament and the second proximal to the popliteal artery. DIDS or DCPIB was injected intramuscularly at a dose of 10 mg/kg (50 μL) after surgery and then continuously administered every other day. The blood flow was recorded on days 1, 7, and 14 post operation using a laser Doppler perfusion imaging analyzer (Moor, Oxford,

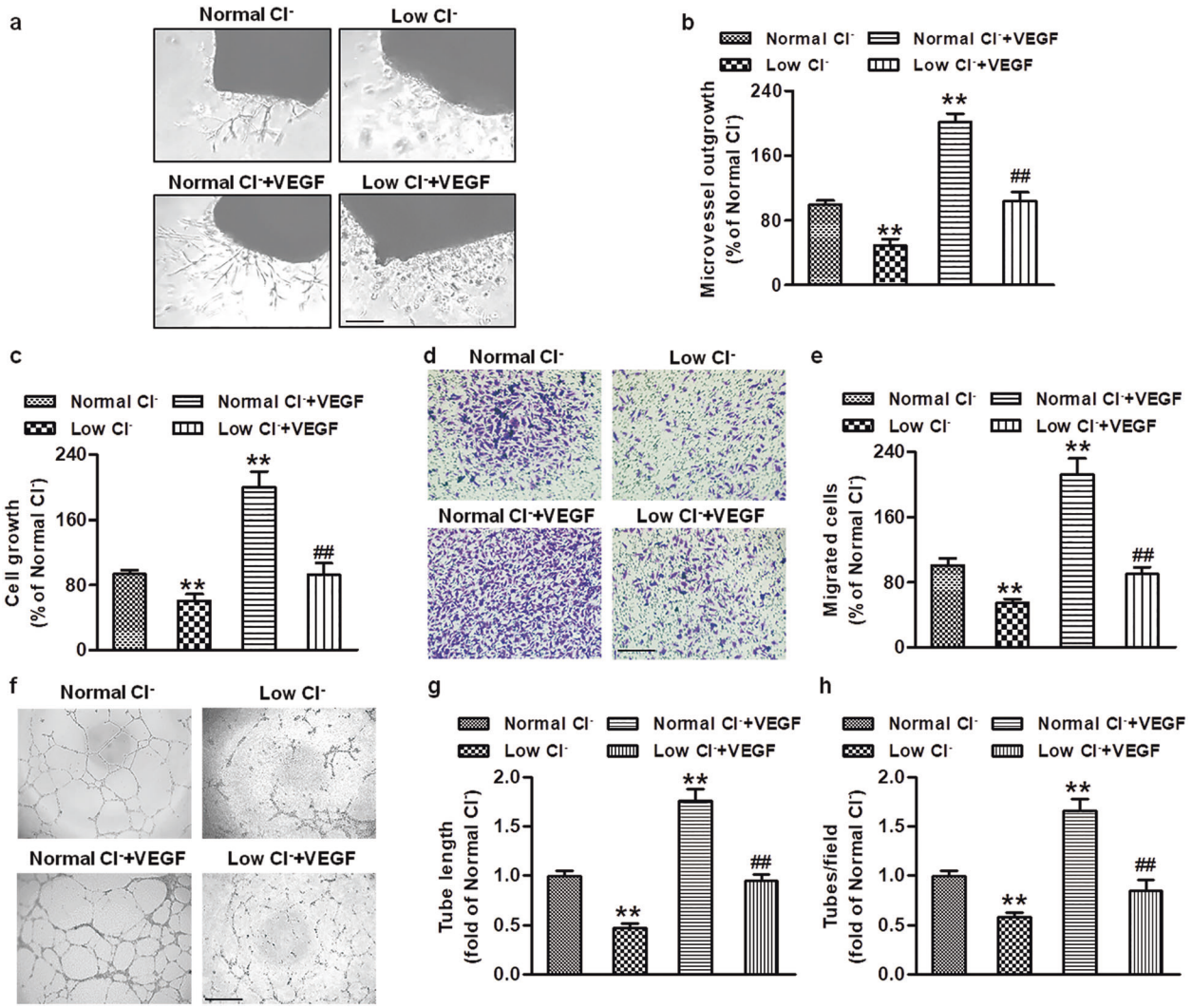

Fig. 1 Reduced $[Cl^-]_i$ inhibits angiogenesis in vitro. a Aortic rings were cultured in normal Cl^- medium or low Cl^- medium in the absence or presence of VEGF (50 ng/mL) for 4 days. Microvessel growth was observed under a microscope. Scale bars = 200 μm. **b** The outgrowth areas were quantified with Image-Pro Plus software. $^{**}P < 0.01$ vs. normal Cl^-; $^{\#\#}P < 0.01$ vs. normal Cl^- + VEGF, $n = 6$. **c** HUVECs were treated with normal Cl^- or low Cl^- medium containing VEGF (50 ng/mL) for 48 h. Cell viability was examined by CCK-8 assays. $^{**}P < 0.01$ vs. normal Cl^-; $^{\#\#}P < 0.01$ vs. normal Cl^- + VEGF, $n = 8$. **d** Cell migration was determined by Transwell analysis. Representative images are shown. Scale bars = 100 μm. **e** Quantitative analysis of the number of migrated cells. $^{**}P < 0.01$ vs. normal Cl^-; $^{\#\#}P < 0.01$ vs. normal Cl^- + VEGF, $n = 5$. **f** Representative images showing endothelial cell tube formation. Scale bars = 200 μm. Quantification of tube length (**g**) and numbers (**h**) was performed by Image-Pro Plus software. $^{**}P < 0.01$ vs. normal Cl^-; $^{\#\#}P < 0.01$ vs. normal Cl^- + VEGF, $n = 6$.

England). The calculated recovery of perfusion is expressed as the ratio of the ischemic hind limb to nonischemic hind limb. All mice were sacrificed at 14 days post operation, and the calf was harvested from the ischemic limbs for histological analysis.

Immunohistochemistry

The calf muscle was fixed with 4% paraformaldehyde and embedded in Tissue-Tek optimal cutting temperature compound (OCT, Sakura, Japan) for sectioning at 5-μm thickness. The sections were pretreated with 5% bovine serum albumin for 30 min to block nonspecific binding and then incubated with CD31 antibody (1:50 dilution; Cambridge, MA, USA) overnight at 4 °C. Following 1 h incubation with biotinylated secondary anti-rabbit antibody at room temperature, the staining was visualized with 3,3'-diaminobenzidine tetrachloride chromogen solution under a light microscope (BX51, Olympus). The number of capillaries was counted in six random fields from each image taken at low magnification (×100) on the tissues, and the density of capillaries is expressed as capillaries per cross section.

Data analysis and statistics

All data are presented as the mean ± standard error of the mean (SEM). The data and statistical analysis comply with recommendations of the *British Journal of Pharmacology* on experimental design and analysis in pharmacology [28, 29]. Statistical comparisons were analyzed by an unpaired two-tailed Student's *t* test or one-way analysis of variance followed by Bonferroni's multiple comparison post hoc test with a 95% confidence interval. All statistical calculations were performed using SPSS 19.0 software (Chicago, IL. USA). $P < 0.05$ was considered to indicate significance. Each experiment was performed at least five times independently.

RESULTS

Lowering $[Cl^-]_i$ inhibits angiogenesis in vitro

To determine whether a reduction in $[Cl^-]_i$ can regulate angiogenesis, we prepared cell culture medium with a reduced Cl^- concentration to decrease $[Cl^-]_i$ as we previously described [18, 19]. Compared with the normal Cl^- medium, the low Cl^-

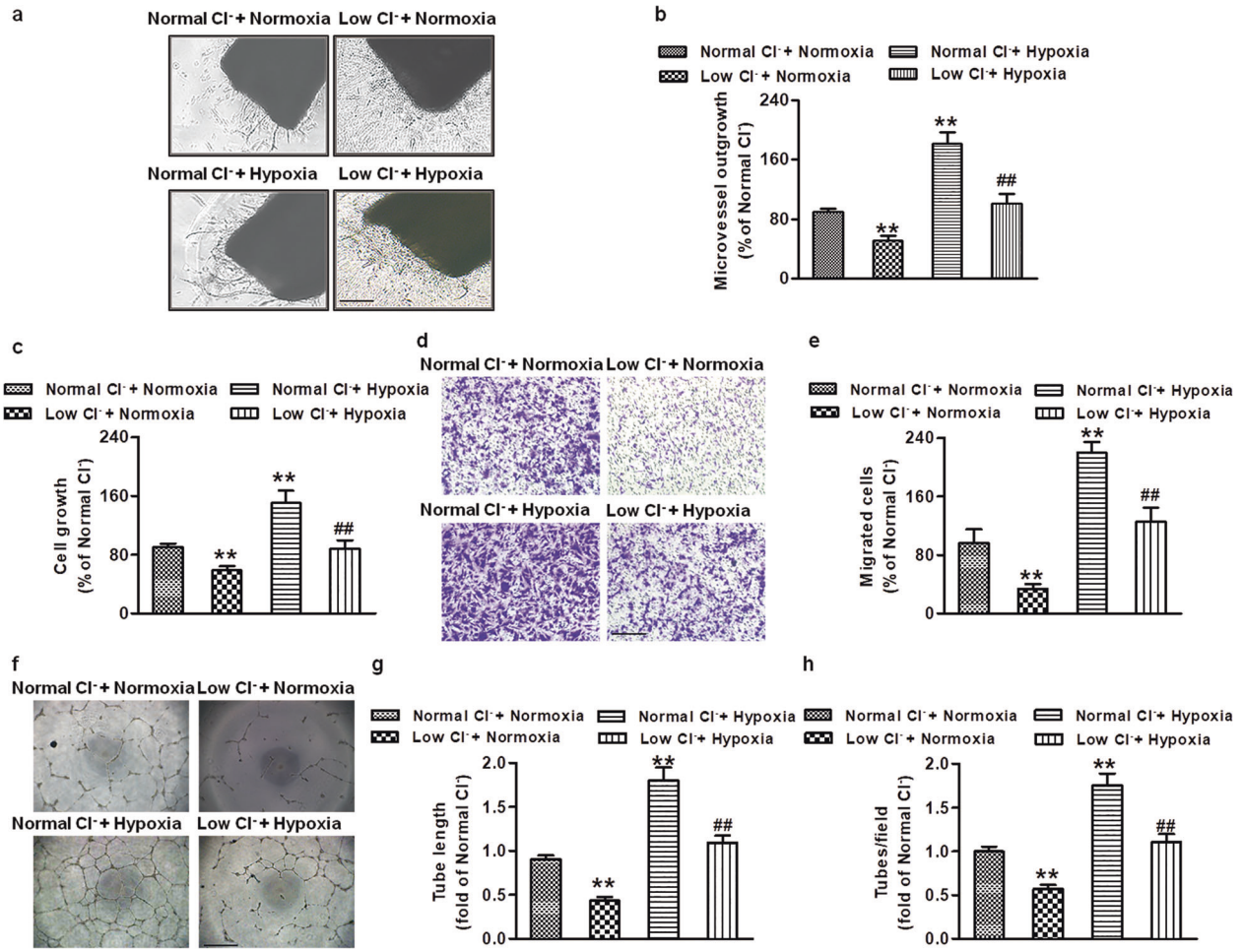

Fig. 2 Low Cl^- inhibits hypoxia-induced angiogenesis in vitro. a Representative phase-contrast micrographs of aortic rings cultured with normal Cl^- or low Cl^- medium for 4 days under normoxic (21% O_2) or hypoxic (1% O_2) conditions. Scale bar = 200 μm. **b** Quantification of vascular outgrowth assessed by Image-Pro Plus software. $^{**}P < 0.01$ vs. normal Cl^- + normoxia; $^{\#\#}P < 0.01$ vs. normal Cl^- + hypoxia, $n = 5$. **c** Cell proliferation of HUVECs was detected by CCK-8 assays. $^{**}P < 0.01$ vs. normal Cl^- + normoxia; $^{\#\#}P < 0.01$ vs. normal Cl^- + hypoxia, $n = 6$. **d** Representative images of the transwell assay to assess HUVEC migration stained by crystal violet under normoxic or hypoxic conditions. Scale bar = 100 μm. **e** The relative migrated cell numbers were quantified by measuring solubilized crystal violet. $^{**}P < 0.01$ vs. normal Cl^- + normoxia; $^{\#\#}P < 0.01$ vs. normal Cl^- + hypoxia, $n = 6$. **f** Representative pictures of HUVEC tube formation under normoxic or hypoxic conditions. Scale bar = 200 μm. Quantification of tube formation assessed by the number of tubes (**g**) and length of tubes (**h**). $^{**}P < 0.01$ vs. normal Cl^- + normoxia; $^{\#\#}P < 0.01$ vs. normal Cl^- + hypoxia, $n = 6$.

medium decreased the $[Cl^-]_i$ from 33.2 to 16.18 mmol/L in HUVECs (Fig. S1). Reduction of $[Cl^-]_i$ significantly decreased the outgrowth area of the aortic ring after 4 days of incubation. VEGF (50 ng/mL) promoted new microvessel growth from the aortic ring, which was substantially inhibited in the low Cl^- medium (Fig. 1a, b). Angiogenesis is a complex process that mainly consists of cell proliferation, migration, and tube formation [3]. As shown in Fig. 1c, a decrease in $[Cl^-]_i$ inhibited the growth of HUVECs under basal conditions. VEGF treatment strongly increased the HUVEC viability, and this increase was attenuated in the low Cl^- medium. Moreover, lowering $[Cl^-]_i$ not only decreased HUVEC migration under basal conditions but also inhibited the VEGF-induced increase in cell migration (Fig. 1d, e). Consistently, the tube formation assay revealed that the formation of a capillary-like network induced by VEGF was also substantially inhibited in the low Cl^- medium (Fig. 1f–h).

Hypoxia has been shown to contribute to the regulation of the growth of new vessels in ischemic diseases [30, 31]. To confirm the effect of Cl^- on hypoxia-induced angiogenesis, we performed aortic ring assays and cultured HUVECs under hypoxic (1% O_2) conditions. Consistent with the aforementioned results, hypoxic (1% O_2) treatment promoted vessel outgrowth in aortic ring assays, while outgrowth from low Cl^--treated aortic rings was weakened (Fig. 2a, b). Similarly, hypoxia-treated HUVEC cultures showed elevated proliferation, migration, and tube formation phenotypes. Low Cl^--treated HUVECs also failed to proliferate (Fig. 2c), migrate (Fig. 2d, e), and form tubes compared with those in normal Cl^- (Fig. 2f–h). Our data demonstrated that low Cl^- also restrained EC proliferation, migration, tube formation, and vessel outgrowth in response to hypoxia.

Low Cl^- medium attenuates the VEGF-induced cytoskeleton reorganization in endothelial cells

Endothelial cell migration is characterized by substantial remodeling of the actin cytoskeleton, which reorganizes into transcytoplasmic stress fibers, along with increased polymerized actin and focal adhesion [32]. To determine whether a decrease in $[Cl^-]_i$ affects cytoskeleton remodeling, we analyzed markers of stress fibers and focal adhesion by immunofluorescence. F-actin staining showed that the number of stress fibers was significantly decreased in the low Cl^- medium. VEGF stimulation led to marked actin remodeling into stress fibers. In contrast, lowering $[Cl^-]_i$ was associated with inhibited formation of stress fibers. Moreover, a decrease in $[Cl^-]_i$ resulted in a decrease in the random

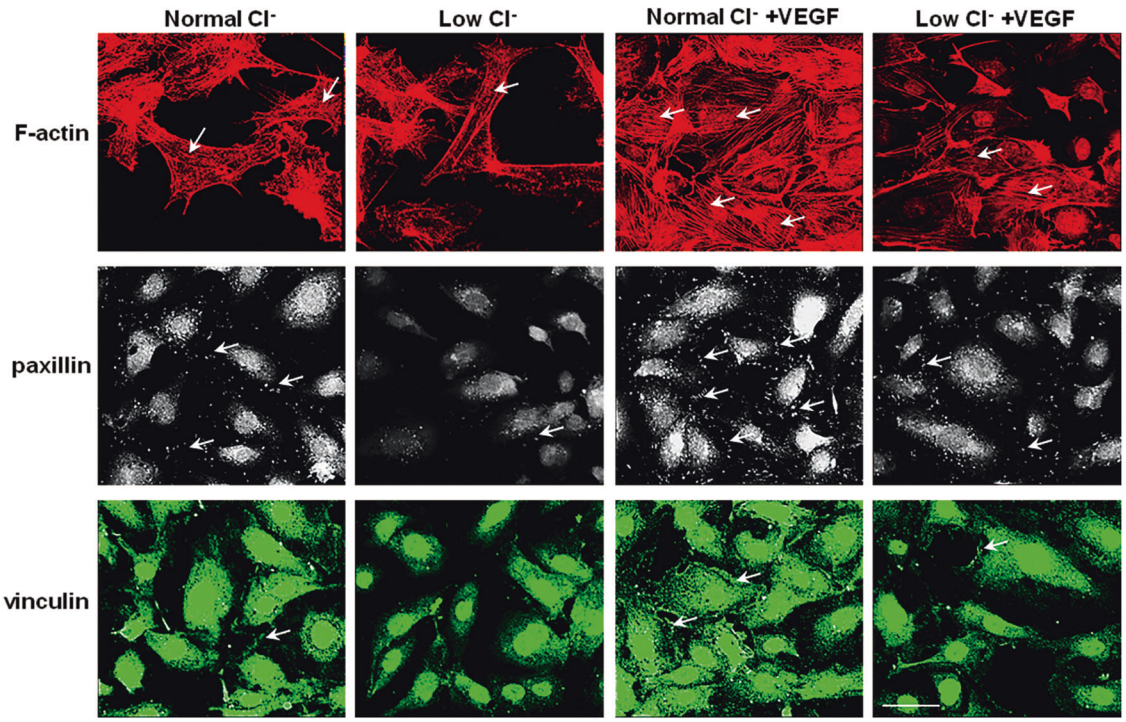

Fig. 3 A decrease in $[Cl^-]_i$ attenuates VEGF-induced cytoskeletal reorganization in HUVECs. The cells were treated with normal Cl^- or low Cl^- medium containing VEGF (50 ng/mL) for 48 h. F-actin was visualized by rhodamine-phalloidin staining. Focal adhesions in HUVECs were observed by immunofluorescence staining using paxillin and vinculin antibodies, respectively. Representative images from five independent experiments are shown. White arrows indicate stress fibers and focal adhesions. Scale bars = 50 μm, $n = 6$.

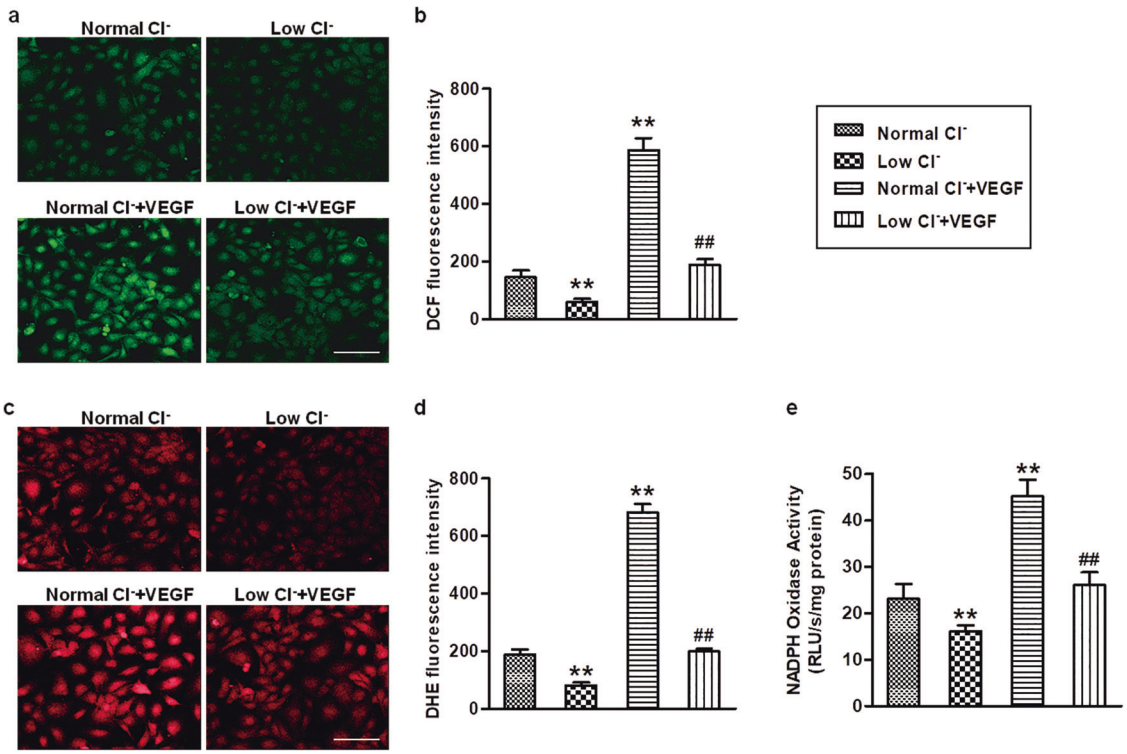

Fig. 4 Reduction of $[Cl^-]_i$ limits ROS generation and NADPH oxidase activity in HUVECs. ROS generation was detected in HUVECs cultured with normal Cl^- and low Cl^- medium by staining with H_2DCF-DA (**a**, **b**) and DHE (**c**, **d**). Representative pictures of H_2DCF-DA (**a**) and DHE (**c**) staining are shown. Scale bars = 200 μm. Quantitative analysis of H_2DCF-DA (**b**) and DHE (**d**) fluorescence intensity. **e** Bar charts showing the activity of NADPH oxidase in HUVECs cultured with normal Cl^- and lower Cl^- medium containing VEGF (50 ng/mL) treatment for 48 h. $^{**}P < 0.01$ vs. normal Cl^-; $^{\#\#}P < 0.01$ vs. normal Cl^- + VEGF, $n = 6$.

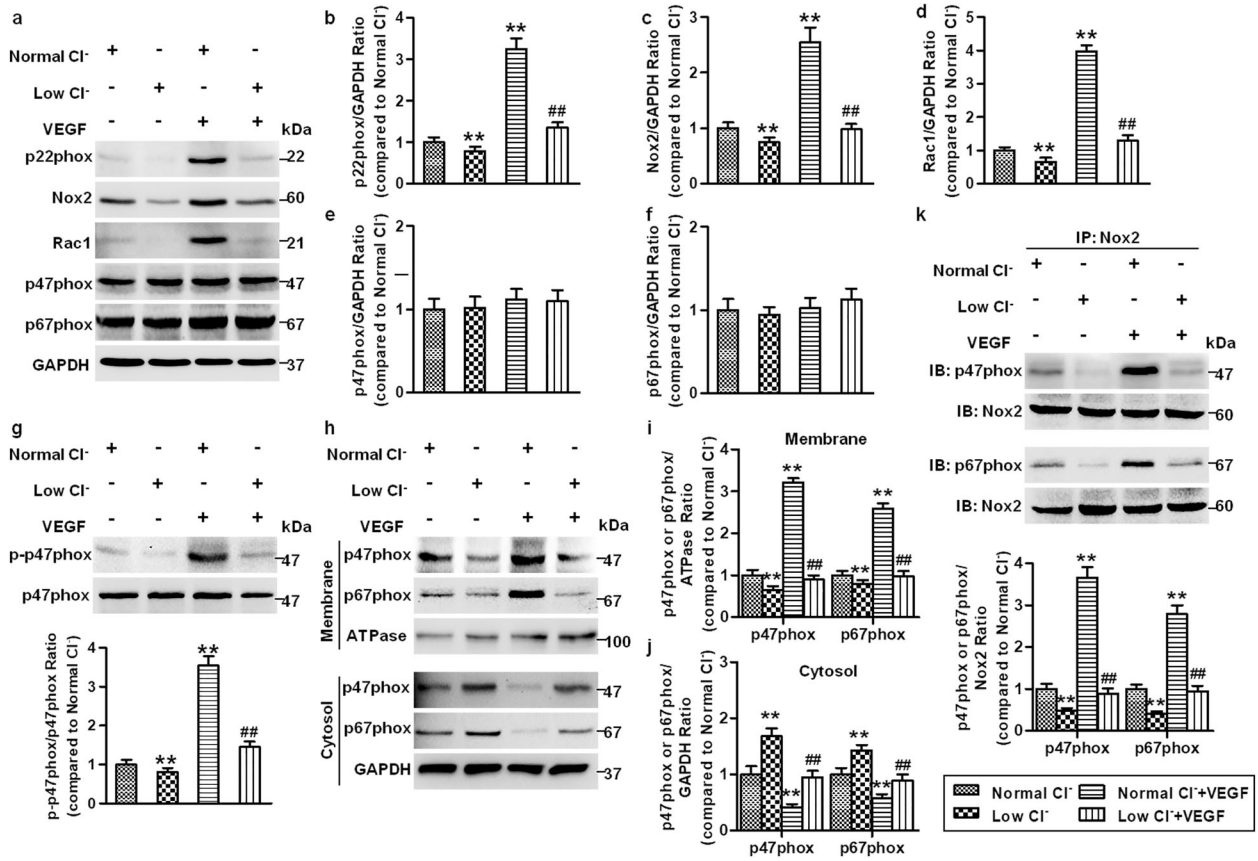

Fig. 5 Reduced $[Cl^-]_i$ decreases the formation of NADPH oxidase complex. a HUVECs were cultured in normal Cl^- and low Cl^- medium containing VEGF (50 ng/mL) for 48 h. The expression of the NADPH oxidase subunits Nox2, p22phox, p47phox, p67phox, and Rac1 was measured in HUVECs. GAPDH was used as a loading control. **b–f** Quantification of the above protein abundance. $^{**}P < 0.01$ vs. normal Cl^-, $^{\#\#}P < 0.01$ vs. normal Cl^- + VEGF, $n = 5$. **g** Cells in normal Cl^- and low Cl^- medium were treated with or without VEGF (50 ng/mL) for 30 min. P47phox phosphorylation and total protein expression were examined. $^{**}P < 0.01$ vs. normal Cl^-; $^{\#\#}P < 0.01$ vs. normal Cl^- + VEGF, $n = 6$. **h** After the treatment described in (**a**), the contents of p47phox and p67phox in the membrane and cytoplasm were detected. Na^+/K^+ ATPase was used as an internal control of the membrane. Quantification of the abundance of p47phox and p67phox in the membrane (**i**) and cytoplasm (**j**). $^{**}P < 0.01$ vs. normal Cl^-; $^{\#\#}P < 0.01$ vs. normal Cl^- + VEGF, $n = 5$. **k** Cell lysates were immunoprecipitated with anti-Nox2 and immunoblotted with anti-p47phox or anti-p67phox. $^{**}P < 0.01$ vs. normal Cl^-; $^{\#\#}P < 0.01$ vs. normal Cl^- + VEGF, $n = 5$.

formation of paxillin-containing focal adhesions. After VEGF stimulation, the increased number of focal adhesions was less pronounced in the low Cl^- medium than in the normal Cl^- medium. In addition, we observed the distribution of vinculin, which is also a prominent member of focal adhesions [32]. VEGF moderately increased the number of focal adhesion junctions at the terminus of short actin bundles. However, in the low Cl^- medium, the staining of vinculin around the cell boundary was significantly decreased (Fig. 3). These results suggest that $[Cl^-]_i$ plays an important role in regulating cytoskeletal organization.

Reduction of $[Cl^-]_i$ blocks ROS generation by suppressing NADPH oxidase activity in endothelial cells

Given the involvement of ROS in angiogenesis [7, 33], we next determined the effects of reduced $[Cl^-]_i$ on the ROS levels in HUVECs. Under basal conditions, lowering $[Cl^-]_i$ slightly inhibited the generation of ROS. Similar to a previous study [33], ROS generation was significantly increased after VEGF treatment. The increased ROS generation in HUVECs was less pronounced in the low Cl^- medium than in the normal Cl^- medium (Fig. 4a–d). NADPH oxidase is a major source of ROS [34]. We therefore examined whether lowering $[Cl^-]_i$ could impact NADPH oxidase activity by using the membrane fractions to exclude other sources of ROS, such as mitochondria-derived ROS, xanthine oxidase and NO synthases [34, 35]. As shown in Fig. 4e, VEGF substantially increased the activity of NADPH oxidase, which was inhibited by the reduction of $[Cl^-]_i$. NADPH oxidase is an enzyme complex that consists of membrane-bound catalytic Nox2 and p22phox and the cytosolic regulatory subunits p47phox, p67phox, and Rac1 [34]. Analysis of the expression profile of these subunits revealed that the expression of Nox2, p22phox, and Rac1 was increased after VEGF treatment. Reduced $[Cl^-]_i$ was associated with reduced expression of the above proteins, not only under basal conditions but also in cells treated with VEGF (Fig. 5a–d). P47phox and p67phox expression was comparable among the four groups (Fig. 5e, f). P47phox phosphorylation triggers p47phox and p67phox translocation from the cytoplasm to the membrane, which is essential for the activation of NADPH oxidase [36]. To further elucidate the mechanism underlying the effect of $[Cl^-]_i$ on NADPH oxidase activation, we initially examined the phosphorylation level of p47phox. The phosphorylation level of p47phox was elevated in the cells stimulated with VEGF. However, reduction of $[Cl^-]_i$ was associated with decreased p47phox phosphorylation (Fig. 5g). Moreover, VEGF strongly promoted the translocation of p47phox and p67phox, as shown by increased levels of p47phox and p67phox in the plasma membrane, which were depressed by lowering $[Cl^-]_i$ (Fig. 5h–j). Similarly, VEGF-induced interactions of Nox2/p47phox and Nox2/p67phox were substantially attenuated by culture with low $[Cl^-]_i$ medium (Fig. 5k). These findings indicate that disruption of NADPH oxidase complex formation may at least

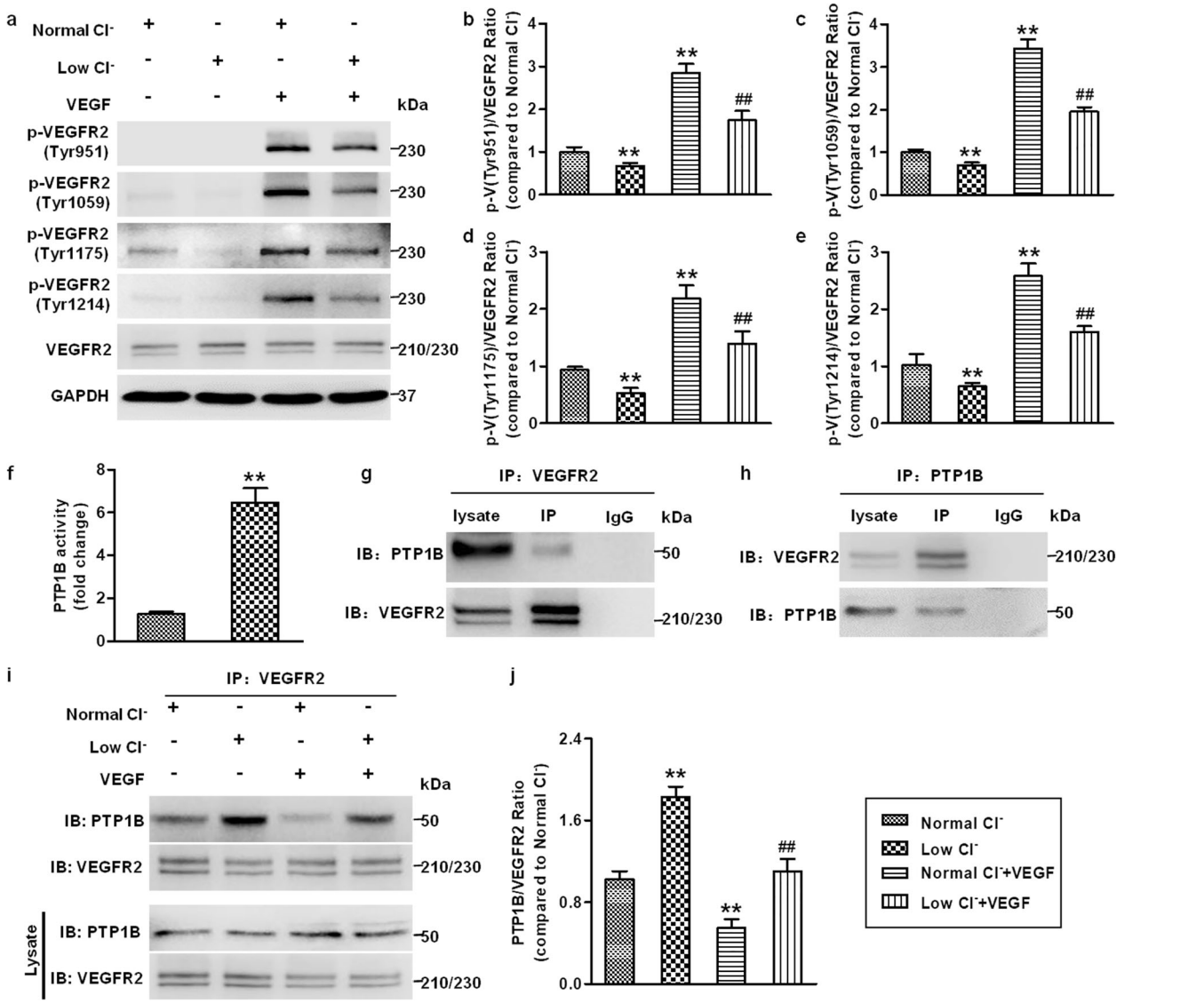

Fig. 6 Lowering $[Cl^-]_i$ impairs VEGFR2 phosphorylation by enhancing PTP1B activity and VEGFR2/PTP1B association. a Western blotting analysis of VEGFR2 phosphorylation at the Tyr951, Tyr1059, Tyr1175, and Tyr1214 sites in HUVECs treated with normal Cl^- and low Cl^- medium followed by VEGF (50 ng/mL) stimulation for 5 min. Densitometric analysis of the phosphorylated levels of VEGFR2 at the Tyr951 (**b**), Tyr1059 (**c**), Tyr1175 (**d**), and Tyr1214 (**e**) sites. $^{**}P < 0.01$ vs. normal Cl^-, $^{\#\#}P < 0.01$ vs. normal Cl^- + VEGF, $n = 6$. **f** HUVECs were incubated with normal Cl^- and low Cl^- medium for 48 h. PTP1B activity was measured. $^{**}P < 0.01$ vs. normal Cl^-, $n = 6$. VEGFR2 interacted with PTP1B. The HUVEC lysates were immunoprecipitated (IP) with VEGFR2 antibody (**g**) or PTP1B antibody (**h**) followed by immunoblotting with PTP1B antibody and VEGFR2 antibody. **i** The cells were treated with normal Cl^- and low Cl^- medium containing VEGF (50 ng/mL) for 48 h. Cell lysates were processed for immunoprecipitation with VEGFR2 antibody, and immunoprecipitated proteins were immunoblotted with PTP1B antibody. **j** Densitometric analysis of the amount of PTP1B in VEGFR2 immunoprecipitates. $^{**}P < 0.01$ vs. normal Cl^-, $^{\#\#}P < 0.01$ vs. normal Cl^- + VEGF, $n = 5$.

partially underlie the inhibitory effect of reduced $[Cl^-]_i$ on ROS generation.

Reduction of $[Cl^-]_i$ inhibits VEGFR2 activation by enhancing PTP1B activity and increasing the binding of VEGFR2 to PTP1B

VEGFR2 is the major mediator required for VEGF signaling activation and VEGF-mediated angiogenesis in vascular endothelial cells [4]. We thus examined the phosphorylation status of VEGFR2. VEGF-induced VEGFR2 Tyr951, Tyr1059, Tyr1175, and Tyr1214 phosphorylation in HUVECs was significantly inhibited in the low Cl^- medium (Fig. 6a–e). It has been suggested that VEGFR2 activity is frequently modulated by binding with multiple key regulatory protein tyrosine phosphatases (PTPs) [37]. PTP1B is a cytoplasmic phosphatase that appears to interact with VEGFR2 and inhibit VEGFR2 phosphorylation and endothelial cell functions [38]. Given the capacity of ROS to regulate PTPs activity [33], together with our aforementioned results showing the effect of lowering $[Cl^-]_i$ on ROS generation and angiogenesis, we investigated whether reduced $[Cl^-]_i$ regulates VEGFR2 activation involving PTP1B. PTP1B activity and the association between VEGFR2 and PTP1B were detected in the low Cl^- medium in the absence or presence of VEGF. Figure 6f shows that PTP1B activity was significantly enhanced under low $[Cl^-]_i$ conditions. Consistent with previous reports [37, 39], a coimmunoprecipitation assay clearly revealed that VEGFR2 interacted with PTP1B (Fig. 6g, h). Importantly, VEGFR2 immunoprecipitation followed by immunoblotting for PTP1B demonstrated that the reduction of $[Cl^-]_i$ enhanced PTP1B coimmunoprecipitation under basal conditions

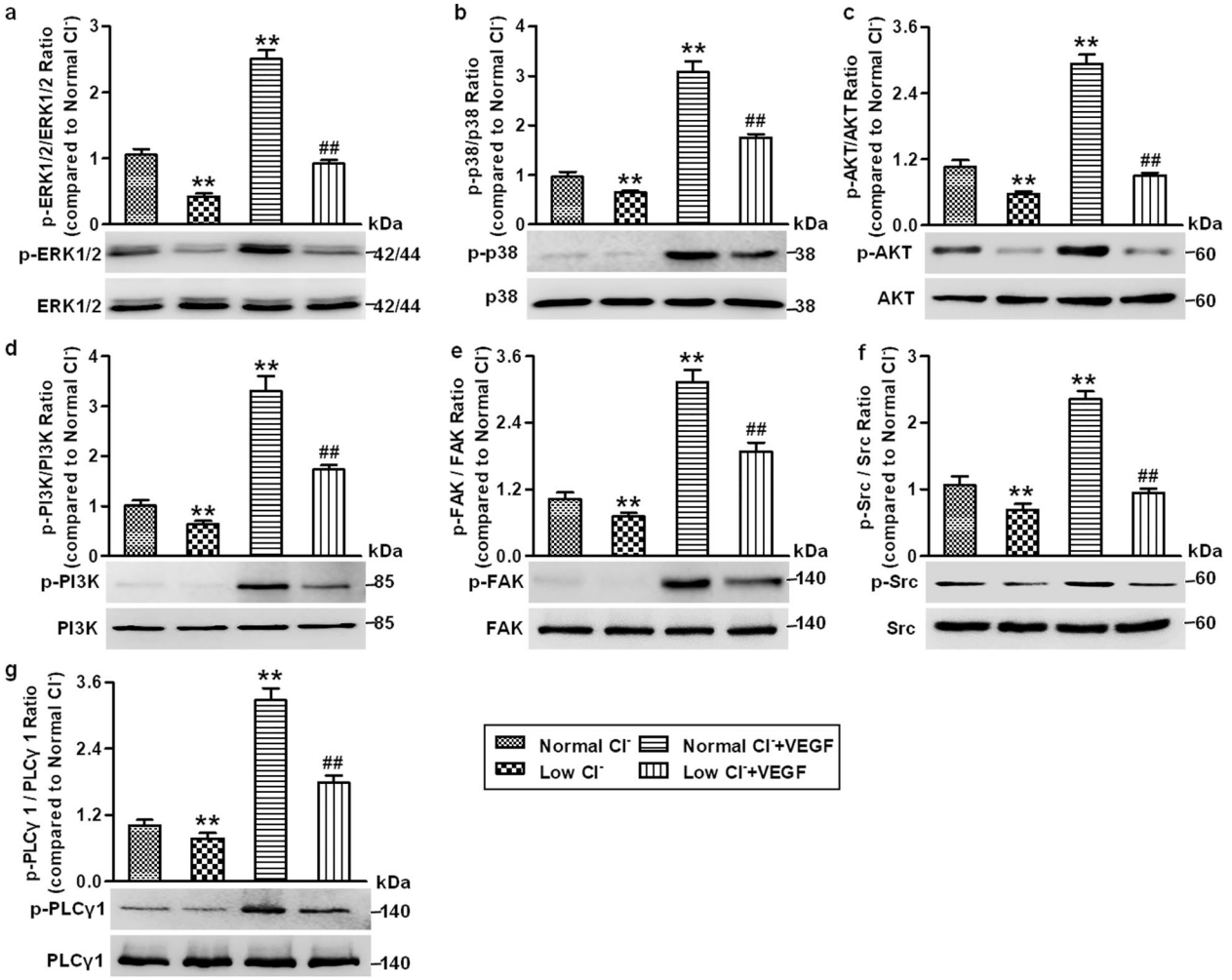

Fig. 7 Low Cl^- medium blocks VEGFR2 downstream axis activation in HUVECs. a–g The cells were cultured in normal Cl^- or low Cl^- medium in the presence or absence of VEGF (50 ng/mL) for 48 h. The phosphorylation of ERK1/2 (**a**), p38 (**b**), AKT (**c**), PI3K (**d**), FAK (**e**), Src (**f**), and PLCγ1 (**g**) was determined by Western blotting. GAPDH was used as a loading control. Densitometric analysis of the phosphorylated levels of the above proteins. $^{**}P < 0.01$ vs. normal Cl^-; $^{\#\#}P < 0.01$ vs. normal Cl^- + VEGF, $n = 6$.

and reversed the VEGF-induced decrease in this interaction (Fig. 6i, j).

Low Cl^- medium suppresses VEGF signaling activation in HUVECs

Similar to the effect of lowering $[Cl^-]_i$ on VEGFR2 phosphorylation, Western blotting analysis of the VEGFR2 downstream axis revealed that the phosphorylation of ERK1/2, p38, AKT, PI3K, FAK, Src, and PLCγ1 was significantly decreased in the low Cl^- medium. VEGF treatment induced a strong increase in the phosphorylation of these kinases, and this increase was substantially attenuated after lowering $[Cl^-]_i$ (Fig. 7), suggesting that reduction of $[Cl^-]_i$ impairs angiogenesis at least by inhibiting VEGF/VEGFR2 signaling activation.

Inhibition of PTPB1 reverses the effect of the low Cl^- medium on angiogenesis

To confirm the critical role of PTP1B in regulating VEGFR2-mediated angiogenesis in low Cl^- medium, we used a PTP1B inhibitor and measured its effects on VEGFR2 phosphorylation and angiogenesis. In the normal Cl^- medium, VEGF-induced phosphorylation of VEGFR2 was significantly potentiated by PTP1B inhibitor II. Moreover, inhibition of PTP1B restored the low Cl^- medium-induced decrease in VEGFR2 phosphorylation under VEGF-treated conditions (Fig. 8a–e). Similarly, the decrease in new microvessel formation in the low Cl^- medium was inhibited after PTP1B inhibition (Fig. 8f, g).

Blockade of Cl^- efflux promotes angiogenesis in the ischemic hind limb of mice

Given that the aforementioned in vitro results showed an inhibitory effect of the low Cl^- medium on angiogenesis, we explored whether inhibition of Cl^- efflux promotes angiogenesis in vivo. VRACs are ubiquitously expressed Cl^- channels and mediate Cl^- efflux [17, 40]. DIDS and DCPIB are specific blockers of VRACs that inhibit Cl^- efflux [17, 19, 41]. Accordingly, the mice were treated with vehicle, DIDS or DCPIB after surgery for hind limb ischemia. Immediately after femoral artery ligation (day 1), blood flow in the ischemic hind limb was decreased equally in all three groups. On postoperative days 7 and 14, blood flow recovery was more pronounced in the DIDS- or DCPIB-treated mice than in the vehicle-treated mice (Fig. 9a, b). Consistently, immunohistochemical staining of the endothelial cell marker CD31 revealed an increased number of capillaries in the calf muscle from the DIDS- or DCPIB-treated mice (Fig. 9c, d). These results indicate that inhibition of Cl^- efflux enhances revascularization of the ischemic hind limb in mice. Moreover, the ROS levels were detected in the model of hind limb ischemia. ROS generation in the ischemic groups was significantly increased compared with

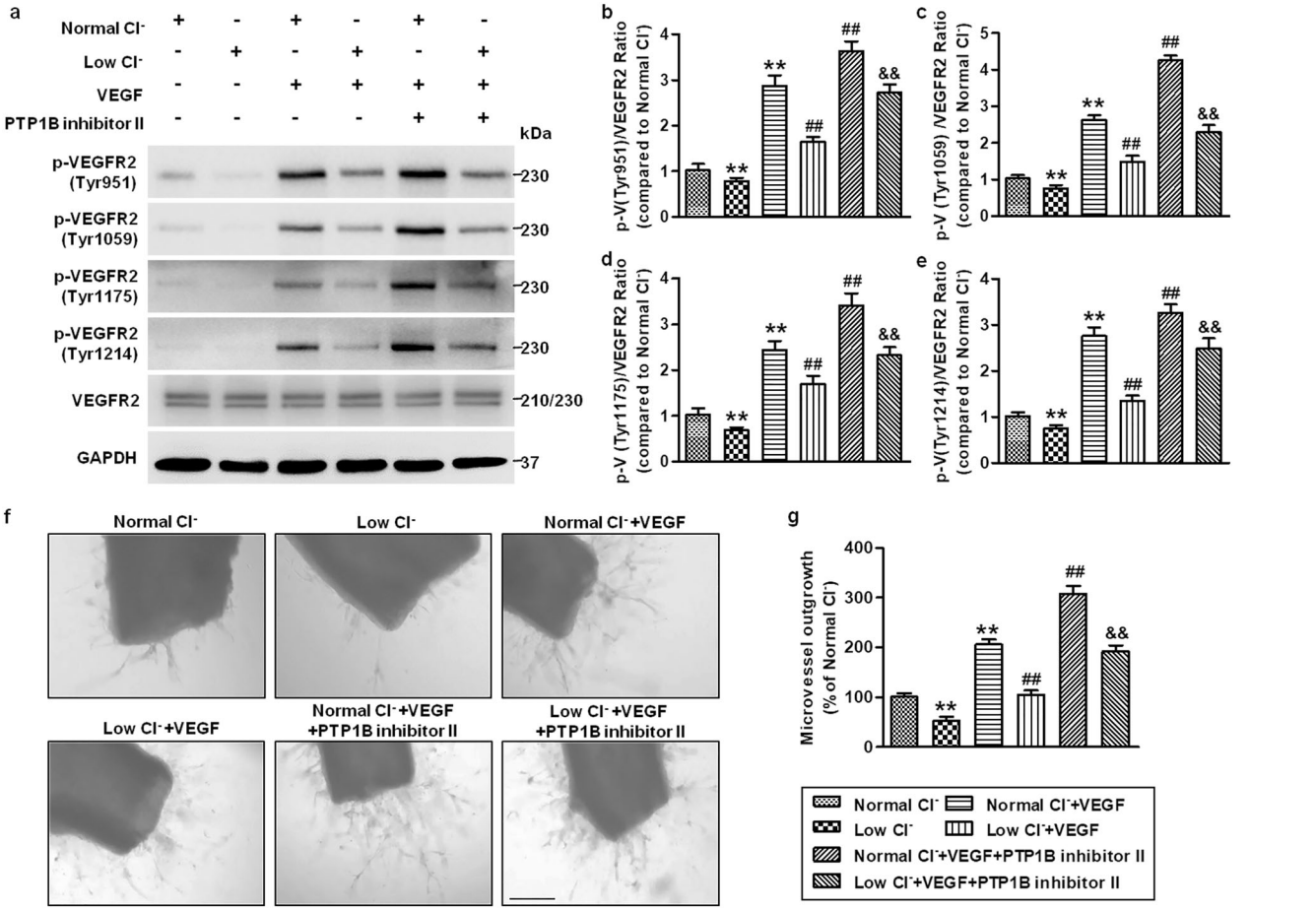

Fig. 8 Pharmacological inhibition of PTP1B reverses the effect of lowering $[Cl^-]_i$ on VEGFR2 phosphorylation and angiogenesis. **a** HUVECs were treated with PTP1B inhibitor II (1 μmol/L) in normal Cl^- or low Cl^- medium for 48 h followed by VEGF (50 ng/mL) stimulation for 5 min. Western blotting analysis of VEGFR2 phosphorylation at the Tyr951, Tyr1059, Tyr1175, and Tyr1214 sites. Representative images are shown. GAPDH was used as a loading control. **b**–**e** Densitometric analysis of the phosphorylated level of VEGFR2 at the Tyr951 (**b**), Tyr1054/1059 (**c**), Tyr1175 (**d**), and Tyr1214 (**e**) sites. $^{**}P < 0.01$ vs. normal Cl^-; $^{\#\#}P < 0.01$ vs. normal Cl^- + VEGF; $^{\&\&}P < 0.01$ vs. low Cl^- + VEGF, $n = 6$. **f** The aortic rings were treated with VEGF (50 ng/mL) and PTP1B inhibitor II (1 μmol/L) in normal Cl^- or low Cl^- medium for 4 days. Microvessel growth was observed under a microscope. Scale bars = 200 μm. **g** Quantification of the outgrowth area. $^{**}P < 0.01$ vs. normal Cl^-; $^{\#\#}P < 0.01$ vs. normal Cl^- + VEGF; $^{\&\&}P < 0.01$ vs. low Cl^- + VEGF, $n = 5$.

that in the sham group. Moreover, treatment with Cl^- channel inhibitors further enhanced the increased generation of ROS (Fig. S2).

DISCUSSION

In this study, we provide clear evidence that Cl^- is a novel regulator of angiogenesis. Reduction of $[Cl^-]_i$ attenuated NADPH oxidase-mediated ROS generation and subsequently reduced VEGFR2 activation by enhancing PTP1B activity and increasing VEGFR2/PTP1B association, leading to suppression of VEGFR2 downstream signaling components, such as PI3K/AKT, Src, FAK, and PLCγ1. These processes together inhibit endothelial cell proliferation, tube formation, migration, and cytoskeleton organization, resulting in angiogenic dysfunction. As such, maintaining $[Cl^-]_i$ homeostasis is critical for angiogenesis and treatment of ischemic diseases.

Alteration of $[Cl^-]_i$ via Cl^- movement across the cell plasma membrane plays an important role in regulating various physiological and pathological processes [13, 18, 19]. Recently, a study showed that hypochloremia is an independent factor of mortality in critically ill patients with septic shock due to the occurrence of metabolic alkalosis [42]. An increased Cl^- level in hypochloremia may decrease the mortality in such patients [42]. Notably, increasing data have shown that serum Cl^- concentration is also involved in the progression of cardiovascular diseases [17–19, 23, 43]. For example, a low serum Cl^- level is regarded as an independent predictor of mortality in patients with hypertension or heart failure [17, 23, 44]. Although our previous work indicated that a decrease in $[Cl^-]_i$ could promote endothelial cell inflammation and foam cell formation [18, 19], the two important pathophysiological features of cardiovascular diseases, the mechanism explaining the higher risk of mortality under a low Cl^- environment remains unclear. Thus, a better understanding of the biological function of Cl^- is warranted.

Given the importance of angiogenesis in ischemic diseases, this study aimed to explore the effect of lowering $[Cl^-]_i$ on angiogenesis. We demonstrated for the first time that a decrease in $[Cl^-]_i$ suppresses angiogenesis in endothelial cells, accompanied by reduced proliferation, migration, capillary-like tube formation, and cytoskeleton reorganization, indicating that increased Cl^- efflux may impair angiogenesis. These findings led us to speculate that blockade of Cl^- efflux could promote neoangiogenesis. Intriguingly, our previous studies have revealed that inhibition of Cl^- efflux with specific VRAC blockers such as DIDS ameliorates vascular inflammation and retards foam cell formation [17, 19]. Moreover, another VARC selective blocker, DCPIB, showed cardioprotective and neuroprotective effects

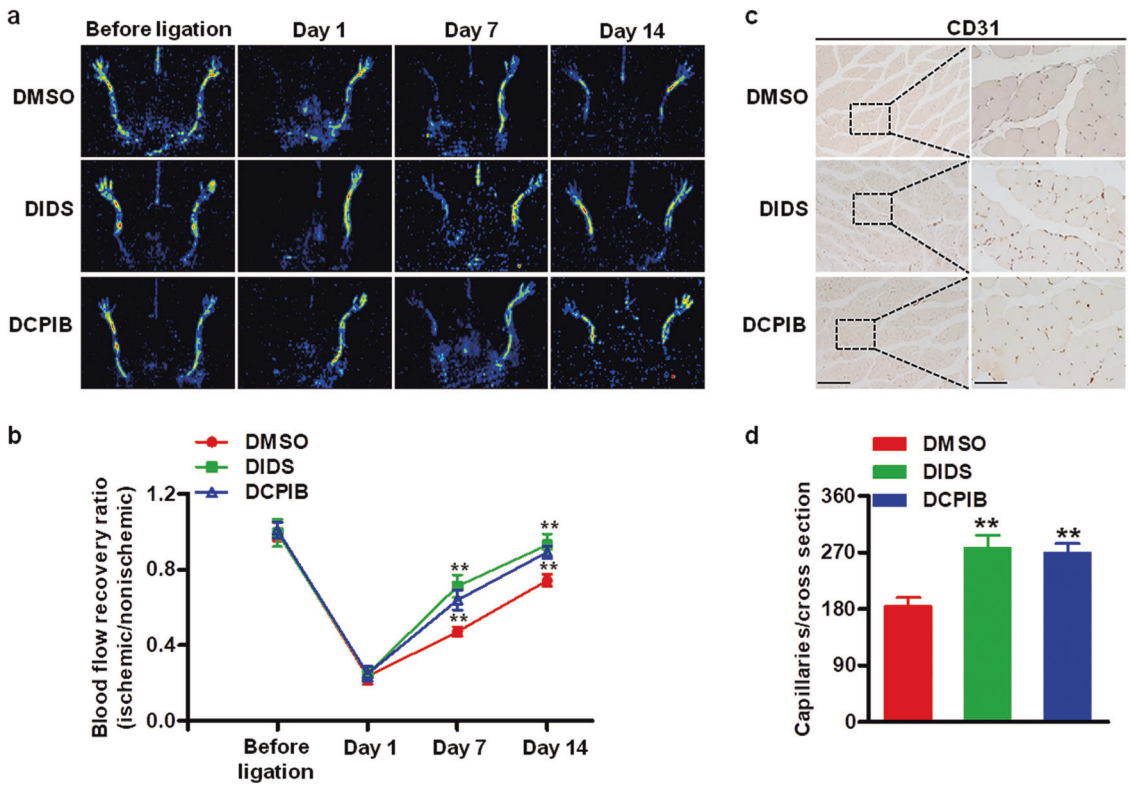

Fig. 9 Inhibition of Cl^- efflux enhances vascularity in hind limb ischemia. a Representative images of hind limb perfusion after inducing hind limb ischemia in the vehicle (DMSO)-, DIDS-, or DCPIB-treated mice. **b** The blood flow of the ischemic hind limb is expressed as the ratio of the ischemic hind limb to the nonischemic hind limb. $^{**}P < 0.01$ vs. DMSO. **c** Representative images of ischemic calf muscle sections from the vehicle (DMSO)-, DIDS-, or DCPIB-treated mice 14 days after surgery that show staining for CD31. Scale bars = 200 μm (left panel) and 50 μm (right panel). **d** Quantification of the number of capillaries. $^{**}P < 0.01$ vs. DMSO, $n = 6$/group.

[41, 45]. In this study, we found that blockade of Cl^- efflux using DIDS or DCPIB effectively enhanced postischemic blood flow perfusion and neoangiogenesis in mice with ischemic hind limbs, further indicating that $[Cl^-]_i$ is an essential modulator of angiogenesis.

VEGF-A primarily binds with VEGFR2 and consequently triggers the dimerization, phosphorylation, and endocytosis of VEGFR2 followed by activation of downstream cascades [1]. Upon VEGF binding to VEGFR2, several tyrosine phosphorylation sites of VEGFR2, such as Tyr951, Tyr1059, Tyr1175, and Tyr1214, are phosphorylated and thus activated [4]. After activation, phosphorylation of VEGFR2 induces the phosphorylation of a series of subsequent tyrosine kinases, such as PI3K-AKT, FAK, Src, PLCγ1, p38, and ERK1/2, which are closely related to cell survival, proliferation, migration, and tube formation [39]. We found that the low Cl^- medium inhibited VEGFR2 phosphorylation at Tyr951, Tyr1059, Tyr1175, and Tyr1214, which led to inactivation of downstream signaling components, including ERK1/2, p38, AKT, PI3K, FAK, Src, and PLCγ1. Pharmacological inhibition of PTP1B with a specific inhibitor through binding to its allosteric site substantially abrogated the effect of low Cl^- medium on angiogenesis. These data suggest that lowering $[Cl^-]_i$ inhibits angiogenesis at least partially by suppressing VEGF/VEGFR2 signaling activation.

Increased ROS levels play an important role in the development of angiogenesis. Angiogenic stress factor-induced ROS generation could promote cell proliferation and migration, cytoskeletal reorganization, and tubular morphogenesis in endothelial cells [35]. In our study, reduced $[Cl^-]_i$ decreased NADPH-mediated ROS generation by decreasing the expression of Nox2, p22phox, and Rac1 and abating the translocation of the cytosolic subunits p47phox and p67phox to the membrane. Interestingly, the signaling properties of ROS are associated with the oxidation of redox-sensitive target proteins such as PTPs, which are enzymes that limit the activity of signaling cascade proteins through dephosphorylation [34]. Tyrosine phosphorylation-mediated intracellular signaling events are usually regulated by PTPs [37, 39]. Notably, several PTPs, such as PTP1B, TC-PTP, VE-PTP, DEP-1/CD148, Src-homology phosphatase-1, and SHP2, have been shown to regulate VEGFR2 activity via dephosphorylation [39]. Among these phosphatases, PTP1B is a nontransmembrane phosphatase that is ubiquitously expressed in various cell types [27, 37]. This molecule dephosphorylates various substrates involved in different signaling pathways, including conventional receptor tyrosine kinases (e.g., epidermal growth factor receptor, platelet derived growth factor receptor, insulin receptor, and insulin-like growth factor receptor) and nonreceptor tyrosine kinases (e.g., c-Src and JAK2) [37]. The functions of PTP1B are primarily focused on the regulation of insulin and leptin receptor activation, which is involved in the development of insulin resistance-related diseases, such as obesity and diabetes [27]. Further, emerging evidence has uncovered the novel functions of PTP1B in cardiovascular diseases. In heart tissues and endothelial cells, PTP1B deficiency was found to improve myocardial ischemia-induced heart failure by enhancing angiogenesis [27, 46, 47]. The effect of PTP1B on angiogenesis is associated with the alteration of VEGF signaling in endothelial cells [2, 46]. Based on these above observations, we explored the involvement of PTP1B in the low Cl^--mediated inhibition of angiogenesis. The results showed that PTP1B activity and the binding of PTP1B to VEGFR2 were strongly potentiated in the low Cl^- solution, indicating that the increased ROS-mediated PTP1B activity may underlie the suppression of VEGFR2 axis activation by lowering $[Cl^-]_i$. In summary, we

demonstrated that a decrease in $[Cl^-]_i$ attenuates NADPH oxidase-derived ROS generation and increases PTP1B activity in endothelial cells, leading to suppression of VEGF/VEGFR2 axis activation and angiogenesis. These findings identify an important role of Cl^- in angiogenesis, suggesting that modulation of $[Cl^-]_i$ may be a novel strategy for the treatment of angiogenic dysfunction-associated diseases, such as myocardial infarction, stroke, and wound healing.

ACKNOWLEDGEMENTS

This work was supported by National Key R&D Program of China (2017YFC0909302), National Natural Science Foundation of China (81525025, 91739104, 81473206, 81930106, 81803519, 81603103, 81603098, 81773723, 81903598), China Postdoctoral Science Foundation (2017M612829, 2018T110917), Natural Science Foundation of Guangdong Province (2019A1515011428, 2018A030310233, 2015A030312009), the Fundamental Research Funds for the Central Universities (19ykpy157, No. 18zxxt74), Science and Technology Program of Guangdong (2015TX01R159, 2015B090903063), and the Science and Technology Program of Guangzhou (201604010087).

AUTHOR CONTRIBUTIONS

JYS, SJL, and JGZ conceived and designed the experiments; KL, YYL, XFL, TTZ, FRZ, JWG, and YH performed the experiments, especially KL, YYL, and XFL carried out most of the experiments; JYS, SJL, KL, YYL, XFL, and QQW analyzed the data; ZML, XL, and XCL contributed reagents/materials/analysis tools. JYS and SJL wrote the paper. All authors participated in the modification of paper.

ADDITIONAL INFORMATION

The online version of this article (https://doi.org/10.1038/s41401-020-0458-7) contains supplementary material, which is available to authorized users.

Competing interests: The authors declare no competing interests.

REFERENCES

1. Patel-Hett S, D'Amore PA. Signal transduction in vasculogenesis and developmental angiogenesis. Int J Dev Biol. 2011;55:353–63.
2. Besnier M, Galaup A, Nicol L, Henry JP, Coquerel D, Gueret A, et al. Enhanced angiogenesis and increased cardiac perfusion after myocardial infarction in protein tyrosine phosphatase 1B-deficient mice. FASEB J. 2014;28:3351–61.
3. Carmeliet P. Angiogenesis in health and disease. Nat Med. 2003;9:653–60.
4. Olsson AK, Dimberg A, Kreuger J, Claesson-Welsh L. VEGF receptor signalling—in control of vascular function. Nat Rev Mol Cell Biol. 2006;7:359–71.
5. Holmstrom KM, Finkel T. Cellular mechanisms and physiological consequences of redox-dependent signalling. Nat Rev Mol Cell Biol. 2014;15:411–21.
6. Kehrer JP, Klotz LO. Free radicals and related reactive species as mediators of tissue injury and disease: implications for Health. Crit Rev Toxicol. 2015;45:765–98.
7. Chiarugi P, Cirri P. Redox regulation of protein tyrosine phosphatases during receptor tyrosine kinase signal transduction. Trends Biochem Sci. 2003;28:509–14.
8. Simons M, Gordon E, Claesson-Welsh L. Mechanisms and regulation of endothelial VEGF receptor signalling. Nat Rev Mol Cell Biol. 2016;17:611–25.
9. Keifer OP, O'Connor DM, Boulis NM. Gene and protein therapies utilizing VEGF for ALS. Pharmacol Ther. 2014;141:261–71.
10. Otrock ZK, Makarem JA, Shamseddine AI. Vascular endothelial growth factor family of ligands and receptors: Review. Blood Cells Mol Dis. 2007;38:258–68.
11. Ivy SP, Wick JY, Kaufman BM. An overview of small-molecule inhibitors of VEGFR signaling. Nat Rev Clin Oncol. 2009;6:569–79.
12. Koch S, Tugues S, Li XJ, Gualandi L, Claesson-Welsh L. Signal transduction by vascular endothelial growth factor receptors. Biochem J. 2011;437:169–83.
13. Nilius B, Droogmans G. Amazing chloride channels: an overview. Acta Physiol Scand. 2003;177:119–47.
14. Chu X, Filali M, Stanic B, Takapoo M, Sheehan A, Bhalla R, et al. A critical role for chloride channel-3 (ClC-3) in smooth muscle cell activation and neointima formation. Arterioscler Thromb Vasc Biol. 2011;31:345–U257.
15. Heimlich G, Cidlowski JA. Selective role of intracellular chloride in the regulation of the intrinsic but not extrinsic pathway of apoptosis in Jurkat T-cells. J Biol Chem. 2006;281:2232–41.
16. Wang XQ, Deriy LV, Foss S, Huang P, Lamb FS, Kaetzel MA, et al. CLC-3 channels modulate excitatory synaptic transmission in hippocampal neurons. Neuron. 2006;52:321–33.
17. Hong L, Xie ZZ, Du YH, Tang YB, Tao J, Lv XF, et al. Alteration of volume-regulated chloride channel during macrophage-derived foam cell formation in atherosclerosis. Atherosclerosis. 2011;216:59–66.
18. Wu QQ, Liu XY, Xiong LX, Shang JY, Mai XY, Pang RP, et al. Reduction of intracellular chloride concentration promotes foam cell formation. Jpn Circ J. 2016;80:1024.
19. Yang H, Huang LY, Zeng DY, Huang EW, Liang SJ, Tang YB, et al. Decrease of intracellular chloride concentration promotes endothelial cell inflammation by activating nuclear factor-kappaB pathway. Hypertension. 2012;60:1287–93.
20. McCallum L, Jeemon P, Hastie CE, Patel RK, Williamson C, Redzuan AM, et al. Serum chloride is an independent predictor of mortality in hypertensive patients. Hypertension. 2013;62:836–43.
21. Cuthbert JJ, Pellicori P, Rigby A, Pan D, Kazmi S, Shah P, et al. Low serum chloride in patients with chronic heart failure: clinical associations and prognostic significance. Eur J Heart Fail. 2018;20:1426–35.
22. Morine KJ, Paruchuri V, Qiao X, Mohammad N, McGraw A, Yunis A, et al. Circulating multimarker profile of patients with symptomatic heart failure supports enhanced fibrotic degradation and decreased angiogenesis. Biomarkers. 2016;21:91–7.
23. Pannella M, Caliceti C, Fortini F, Aquila G, Vieceli Dalla Sega F, Pannuti A, et al. Serum from advanced heart failure patients promotes angiogenic sprouting and affects the notch pathway in human endothelial cells. J Cell Physiol. 2016;231:2700–10.
24. Yi T, Yi Z, Cho SG, Luo J, Pandey MK, Aggarwal BB, et al. Gambogic acid inhibits angiogenesis and prostate tumor growth by suppressing vascular endothelial growth factor receptor 2 signaling. Cancer Res. 2008;68:1843–50.
25. Yu BX, Yuan JN, Zhang FR, Liu YY, Zhang TT, Li K, et al. Inhibition of Orai1-mediated Ca(2+) entry limits endothelial cell inflammation by suppressing calcineurin-NFATc4 signaling pathway. Biochem Biophys Res Commun. 2018;495:1864–70.
26. Nakamura Y, Patrushev N, Inomata H, Mehta D, Urao N, Kim HW, et al. Role of protein tyrosine phosphatase 1B in vascular endothelial growth factor signaling and cell-cell adhesions in endothelial cells. Circ Res. 2008;102:1182–91.
27. Lanahan AA, Lech D, Dubrac A, Zhang J, Zhuang ZW, Eichmann A, et al. PTP1b is a physiologic regulator of vascular endothelial growth factor signaling in endothelial cells. Circulation. 2014;130:902–9.
28. Curtis MJ, Bond RA, Spina D, Ahluwalia A, Alexander SP, Giembycz MA, et al. Experimental design and analysis and their reporting: new guidance for publication in BJP. Br J Pharmacol. 2015;172:3461–71.
29. Curtis MJ, Alexander S, Cirino G, Docherty JR, George CH, Giembycz MA, et al. Experimental design and analysis and their reporting II: updated and simplified guidance for authors and peer reviewers. Br J Pharmacol. 2018;175:987–93.
30. Eltzschig HK, Bratton DL, Colgan SP. Targeting hypoxia signalling for the treatment of ischaemic and inflammatory diseases. Nat Rev Drug Discov. 2014;13:852–69.
31. Semenza GL. Hypoxia-inducible factor 1 and cardiovascular disease. Annu Rev Physiol. 2014;76:39–56.
32. Huveneers S, Oldenburg J, Spanjaard E, van der Krogt G, Grigoriev I, Akhmanova A, et al. Vinculin associates with endothelial VE-cadherin junctions to control force-dependent remodeling. J Cell Biol. 2012;196:641–52.
33. Sprott D, Poitz DM, Korovina I, Ziogas A, Phieler J, Chatzigeorgiou A, et al. Endothelial-specific deficiency of ATG5 (autophagy protein 5) attenuates ischemia-related angiogenesis. Arterioscler Thromb Vasc Biol. 2019;39:1137–48.
34. Ushio-Fukai M. Redox signaling in angiogenesis: role of NADPH oxidase. Cardiovasc Res. 2006;71:226–35.
35. Ma MM, Gao M, Guo KM, Wang M, Li XY, Zeng XL, et al. TMEM16A contributes to endothelial dysfunction by facilitating Nox2 NADPH oxidase-derived reactive oxygen species generation in hypertension. Hypertension. 2017;69:892.
36. Bedard K, Krause KH. The NOX family of ROS-generating NADPH oxidases: physiology and pathophysiology. Physiol Rev. 2007;87:245–313.
37. Stuible M, Tremblay ML. In control at the ER: PTP1B and the down-regulation of RTKs by dephosphorylation and endocytosis. Trends Cell Biol. 2010;20:672–9.
38. Nakamura Y, Patrushev N, Inomata H, Mehta D, Urao N, Kim HW, et al. Role of protein tyrosine phosphatase 1B in vascular endothelial growth factor signaling and cell-cell adhesions in endothelial cells. Circ Res. 2008;102:1182–91.
39. Nie L, Guo X, Esmailzadeh L, Zhang J, Asadi A, Collinge M, et al. Transmembrane protein ESDN promotes endothelial VEGF signaling and regulates angiogenesis. J Clin Investig. 2013;123:5082–97.
40. Zhou JG, Ren JL, Qiu QY, He H, Guan YY. Regulation of intracellular Cl^- concentration through volume-regulated ClC-3 chloride channels in A10 vascular smooth muscle cells. J Biol Chem. 2005;280:7301–8.
41. Zhang Y, Zhang H, Feustel PJ, Kimelberg HK. DCPIB, a specific inhibitor of volume regulated anion channels (VRACs), reduces infarct size in MCAo and the release of glutamate in the ischemic cortical penumbra. Exp Neurol. 2008;210:514–20.

42. Oh HJ, Kim SJ, Kim YC, Kim EJ, Jung IY, Oh DH, et al. An increased chloride level in hypochloremia is associated with decreased mortality in patients with severe sepsis or septic shock. Sci Rep. 2017;7:15883.
43. Grodin JL, Simon J, Hachamovitch R, Wu YP, Jackson G, Halkar M, et al. Prognostic role of serum chloride levels in acute decompensated heart failure. J Am Coll Cardiol. 2015;66:659–66.
44. Grodin JL, Verbrugge FH, Ellis SG, Mullens W, Testani JM, Tang WH. Importance of abnormal chloride homeostasis in stable chronic heart failure. Circ Heart Fail. 2016;9:e002453.
45. Wang L, Shen M, Guo X, Wang B, Xia Y, Wang N, et al. Volume-sensitive outwardly rectifying chloride channel blockers protect against high glucose-induced apoptosis of cardiomyocytes via autophagy activation. Sci Rep. 2017;7:44265.
46. Wang Y, Yan F, Ye Q, Wu X, Jiang F. PTP1B inhibitor promotes endothelial cell motility by activating the DOCK180/Rac1 pathway. Sci Rep. 2016;6:24111.
47. Zhang Y, Li Q, Youn JY, Cai H. Protein phosphotyrosine phosphatase 1B (PTP1B) in calpain-dependent feedback regulation of vascular endothelial growth factor receptor (VEGFR2) in endothelial cells: implications in VEGF-dependent angiogenesis and diabetic wound healing. J Biol Chem. 2017;292:407–16.